Macromolecular Journals

Macromolecular Materials and Engineering

Encapsulation of Organic Pigment Particles Via Miniemulsion Polymerization

Nico Steiert, Katharina Landfester*

Different organic yellow, magenta, and blue pigment nanoparticles can be efficiently encapsulated by cosonicating pigment dispersions and monomer miniemulsions in the pigment to monomer weight ratio of 80:20, followed by polymerization. As polymers polystyrene, different polyacrylates or copolymers could be used. Efficient encapsulation was proven by means of ultracentrifugation, electron microscopic methods, and streaming potential titration. Comparing the reaction kinetics of a typical styrene miniemulsion polymerization with the corresponding "ad-miniemulsion polymerizations" proceeding on the surface of pigment particles, an influence of the pigments' molecular structure was observed.

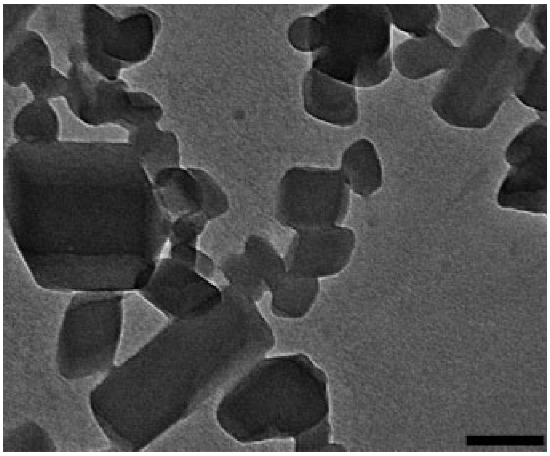

Introduction

Organic pigments have numerous applications in coatings, printing, and paint industries and are of particular interest because of their photosensitivity, color strength, and overall stability. They can be applied as aqueous dispersions. However, after dispersing the water-insoluble pigments in the aqueous phase, they often tend to agglomeration. The coating of organic pigment-nanoparticles with polymer can solve this problem and also protect them from unwanted environmental influences like UV radiation or pH. Moreover, the coating leads to better storage stability, color stability and durability, and the film formation can be adjusted. Therefore, polymer-encapsulated pigments could also find applications in water-based inks.

In the last 10–20 years, many techniques for encapsulating nanoparticles have been developed, for example emulsion, dispersion, and miniemulsion polymerization. A nice overview is given in ref.[1]

One widespread method for encapsulating particles, for example colloidal silica,[2,3] titanium dioxide pigments,[4] and silver particles,[5] using several polymers, is the conventional emulsion polymerization. Besides the difficulty in controlling the dispersion stability of inorganic particles in the aqueous phase prior to polymerization resulting in large aggregates, it is also difficult to ensure, that the polymerization takes place exclusively on the nanoparticles' surface. Due to the complexity of the particle nucleation mechanism, the process often leads to insufficient encapsulation efficiencies. In emulsion polymerization, depending on the water-solubility of the monomer and the amount of surfactant, the main locus for particle nucleation is predominantly either in the aqueous phase, which is called homogeneous nucleation, possibly leading to the formation of new particles during the polymerization, or in the monomer swollen micelles,

N. Steiert, K. Landfester
Institute of Organic Chemistry III – Macromolecular Chemistry and Organic Materials, University of Ulm, Albert-Einstein-Allee 11, 89081 Ulm, Germany
E-mail: katharina.landfester@uni-ulm.de

Macromol. Mater. Eng. **2007**, *292*, 1111–1125

DOI: 10.1002/mame.200700138

called micellar nucleation, where large monomer droplets serve as reservoirs, which feed monomer to the polymerizing particles by diffusing through the aqueous phase. Differences in the diffusion behavior of the relatively water-insoluble monomers from non-polymerizing droplets to growing polymerizing particles can cause variations in the copolymer composition aside from the differences in the reactivity of the comonomers.

Encapsulation of hydrophilic pigments can be achieved by surface modification in terms of hydrophobization prior to polymerization. One possibility of functionalization is the coating with a coupling agent like 3-(trimethoxysilyl) propyl methacrylate (MPS) through surface chemical reaction, as done by Espiard and Guyot, who encapsulated MPS-functionalized silica with poly(ethyl acrylate).[3] MPS enhances the adsorption of non-polar monomer and/or polymer on the mineral surface and also contains a polymerizable olefinic group, providing a covalent attachment of many formed polymer chains to the pigment surface. Functionalization can also be performed through simple adsorption methods, e.g., of cationic initiators such as 2,2′-azobis(2-amidinopropane) dihydrochloride (AIBA·2HCl), which strongly adsorb to negatively charged surfaces. The polymerization reaction of monomers can then be initiated by the initiator molecules AIBA being located at the negatively charged surface, for instance of titanium dioxide particles.[4]

Encapsulation can also be obtained using the dispersion polymerization technique. For example, MPS-coupled silica particles can be encapsulated with polystyrene in aqueous ethanol[6–8] and with poly(*tert*-butyl acrylate) in 2-propanol,[9] respectively.

Miniemulsion polymerization offers several advantages compared to emulsion and dispersion polymerization. Miniemulsions are critically stabilized dispersions, consisting of droplets in the range of 50–500 nm in diameter. Direct (oil-in-water) miniemulsions can be obtained by shearing a system consisting of oil, water, surfactant, and a hydrophobe like hexadecane. The hydrophobe guarantees stabilization of the miniemulsion against diffusion degradation, the so-called Ostwald ripening.[10] Compared to emulsion polymerization, the monomer droplets are small, so that the polymerization occurs by radical entry into the preexisting miniemulsion droplets, called droplet nucleation, without the formation of new particles. During the polymerization, the generated homogeneous monomer droplets keep their particular identity without serious exchange kinetics being involved.[11] As a result, in case of copolymerization, the polymer composition in each particle reflects that of the corresponding monomers in the original droplets. The introduction of species such as pigments into the monomer prior to miniemulsification in the water phase and polymerization leads to high encapsulation efficiencies. Encapsulation of pigments with polymer using the miniemulsion polymerization technique offers the ability to control the droplet size, having the pigment particles directly dispersed in the oil phase, and to nucleate all of the monomer droplets containing the pigment particles.

Using the miniemulsion approach, nanoparticles being more hydrophobic than the monomer can be dispersed in the monomer phase without any former treatment, as recently described for the polystyrene encapsulation of organic phthalocyanine blue pigments[12] or carbon black particles.[13] For the encapsulation of hydrophilic nanoparticles like calcium carbonate,[13] titanium dioxide,[14–16] magnetite,[17] or silica[18] with hydrophobic polymers, hydrophobization is necessary prior to or during the introduction in the monomer phase. Calcium carbonate[13] and magnetite particles[17] can be encapsulated into polystyrene particles using stearic acid and oleoyl sarcosine acid, respectively as hydrophobizing agents. Erdem et al. described the usage of OLOA 370, a polybutene-succinimide pentamine, for successfully dispersing titanium dioxide nanoparticles in organic media.[14] Silica surfaces can be hydrophobized by cetyltrimethylammonium chloride (CTMA-Cl) before the immersion in hydrophobic monomers.[18] However, using the approach of dispersing inorganic material into the monomer phase prior to miniemulsification, only low contents of inorganic material in the resulting nanocomposites can be obtained, and its distribution is usually inhomogeneous.

Therefore, a new route for the production of polymer-encapsulated hydrophobic particles has been developed which is also based on miniemulsion processes. The cosonication of nanoparticle dispersion and monomer miniemulsion followed by polymerization leads to effective particle encapsulation. It was shown, that using this method, hydrophobic carbon black particles can be encapsulated with polystyrene very efficiently, varying the ratio of carbon black to polymer over a wide range.[19] The polymerization can be described as polymerization in an adsorbed monomer layer created and stabilized as miniemulsion (‘‘ad-miniemulsion polymerization’’). Using the same encapsulation method, hydrophobized magnetite can be encapsulated resulting in particles of high homogeneity with up to 40 wt.-% of magnetite.[20]

This paper deals with polymer encapsulation of different organic pigment nanoparticles by cosonication, resulting in hybrid structures of 80% pigment and 20% polymer. In order to start the radical polymerization in the monomer droplets, an oil-soluble initiator is used. Polystyrene encapsulation is obtained by using an anionic surfactant sodium dodecyl sulfate (SDS) and successful encapsulation is subsequently shown by means of ultracentrifugation, electron microscopic methods, and streaming potential titrations at different pH values.

As the polymerization is expected to take place on the pigment particles' surface, the influence of the kind of pigment in terms of its molecular structure on the polymerization kinetics was calorimetrically analyzed.

Furthermore, in the encapsulation process of the magenta-colored quinacridone pigment, both the type of surfactant and monomer were varied. Polystyrene encapsulation could also be successfully achieved using the cationic surfactant CTMA-Cl and non-ionic surfactant Lutensol AT50 [a poly(ethylene oxide) hexadecyl ether with an EO block length of about 50 units].

Besides polystyrene, encapsulation was also performed with polymers having a low glass transition temperature, such as poly(butyl acrylate) (PBA) or poly(butyl methacrylate) (PBMA), and with the more hydrophilic poly (methyl methacrylate) (PMMA), particularly to arise the polarity of the pigments' surface for further interaction for possible applications in ink-jet printing. Moreover, encapsulation with copolymers of styrene and the analogous acrylates is also described.

Experimental Part

Materials

The monomers [styrene (STY, 99%+, Merck), methyl methacrylate (MMA, 99%+, Merck), butyl acrylate (BA, 99%+, Merck), and butyl methacrylate (BMA, 99%, Aldrich)] were distilled under vacuum and kept under refrigeration until use. The surfactants SDS (99%, Lancester), Lutensol AT50 (BASF), CTMA-Cl (98%+, Fluka), the initiators 2,2′-azobis(2-methylpropionitrile) (AIBN, 98%, Aldrich), 2,2′-azobis(2-methylbutyronitrile) (V-59, Wako), and the hydrophobe hexadecane (99%, Merck) were used as received.

The SDS-stabilized dispersions of the azo pigment yellow 74 (PY74), the quinacridone pigment violet 19 (PV19), and the organic copper phthalocyanine pigment blue 15:3 (PB15:3) (Table 1) were used as supplied by Clariant. In this paper, the pigment contents are always given to the total quantity and the surfactant contents to the amount of pigment. The chemical structure of the pigments is shown in Figure 1.

Synthesis

Preparation of Other Pigment Dispersions Used for Encapsulation

The cationically stabilized dispersion of magenta quinacridone pigment PV19 (Table 1) was prepared by adding a solution of 3.75 g (25.0 wt.-%) CTMA-Cl in 131.25 g water to 15 g (10 wt.-%) pigment PV19, stirring the mixture at 800 rpm overnight, and homogenizing it with an ultraturrax (IKA-Ultra-Turrax T25 basic, shaft type S25 N – 18G) at 24 000 rpm for 15 min and pulsed sonication for 90 min net at 90% amplitude. All sonication processes mentioned in this paper were done with 5 s pulse on and 10 s pulse off cycles under ice-cooling, using an ultrasonic Branson Digital Sonifier 450-D and a 1/2 inch tip.

Non-ionically stabilized dispersions of yellow azo pigment PY74 with Lutensol AT50 contents between 30 and 100 wt.-% (Table 1) were produced by dissolving different amounts of Lutensol AT50 in a pigment dispersion composed of 10 wt.-% pigment PY74 and 15 wt.-% Lutensol AT50, as supplied by Clariant.

Non-ionically stabilized dispersions of magenta quinacridone pigment PV19 with Lutensol AT50 contents between 30 and 100 wt.-% (Table 1) were prepared by adding 90 g of different concentrated aqueous solutions of Lutensol AT50 to 10 g (10 wt.-%) of pigment in each case, stirring the mixtures at 800 rpm overnight, homogenizing them with the ultraturrax at 24 000 rpm for 15 min, and pulsed sonication for 90 min net at 90% amplitude.

Encapsulation Processes

Synthesis of Polystyrene-Encapsulated Pigments Using Anionic Surfactant SDS or Cationic Surfactant CTMA-Cl

For the synthesis of the miniemulsions, an oil phase consisting of 6 g styrene, 250 mg hexadecane and 250 mg oil-soluble azo initiator AIBN was mixed with a surfactant solution of 72 mg anionic SDS or cationic CTMA-Cl in 24 g water. After powerfully stirring the mixtures at 1 500 rpm for 1 h for pre-emulsification, the miniemulsions were prepared by pulse sonicating the emulsions for 2 min net at 90% amplitude.

Table 1. Characteristics of the pigment dispersions used for encapsulation.

Pigment						Surfactant	
Color	**Type**	**Density**	**Particle diameter**[a]	**PDI**[a]	**Content**[b]	**Type**	**Content**[c]
		$g \cdot cm^{-3}$	**nm**		**wt.-%**		**wt.-%**
Yellow	PY74	1.41	132	0.316	17.0	SDS	8.8
Yellow	PY74	1.41	143	0.242	9.2–9.9	Lutensol AT50	30.0–100.0
Magenta	PV19	1.47	89	0.181	20.0	SDS	17.5
Magenta	PV19	1.47	99	0.254	10.0	CTMA-Cl	25.0
Magenta	PV19	1.47	94	0.211	10.0	Lutensol AT50	30.0–100.0
Cyan blue	PB15:3	1.61	112	0.290	17.0	SDS	17.6

[a] Determined by DLS; [b] Related to total quantity; [c] Related to pigment.

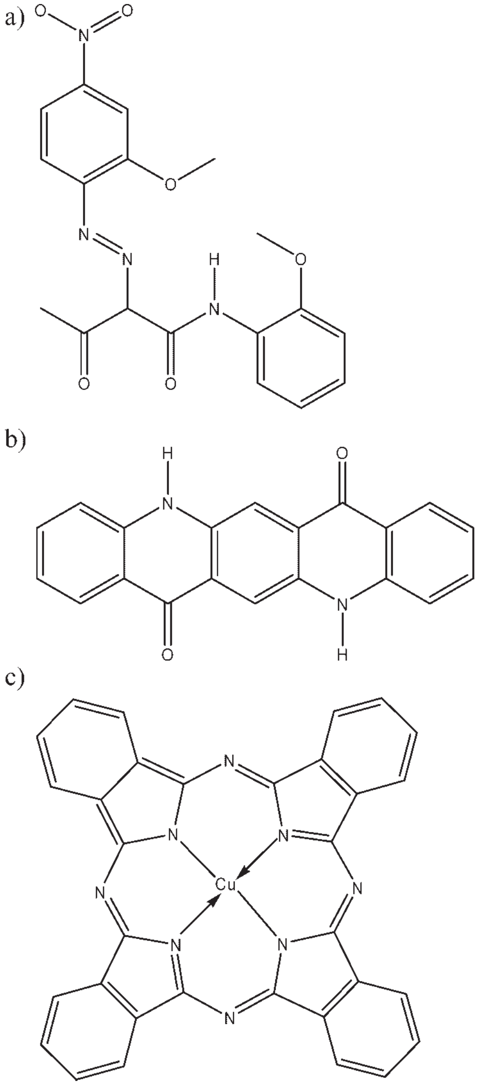

Figure 1. Chemical structures of (a) the yellow azo pigment PY74; (b) the magenta quinacridone pigment PV19; and (c) the cyan blue organic copper phthalocyanine pigment PB15:3.

The anionic dispersions of PY74, PV19, and PB15:3 stabilized by SDS, and the cationic dispersion of PV19, stabilized by CTMA-Cl, were used for encapsulation. To 25 g of the different pigment dispersions was given, in each case, the amount of miniemulsion that corresponds to the weight ratio of pigment to monomer of 80:20. The added miniemulsion was always stabilized by the same surfactant like the pigment dispersion.

The dispersions were powerfully stirred at 1 500 rpm for 30 min, pulse sonicated for 2 min net at 50% amplitude, again stirred at 1 500 rpm for 40 min and finally pulse sonicated for 2 min net at 70% amplitude. In order to prevent pre-polymerization of monomer during the sonication processes, sonication was performed with 5 s pulse on and 10 s pulse off cycles under ice-cooling within all encapsulation processes described in this paper. Finally, polymerization was performed at 72 °C overnight. To achieve a complete polymerization, the gas room of the reaction flask was minimized.

Synthesis of Polystyrene-Encapsulated Pigments Using Non-Ionic Surfactant Lutensol AT50

For the synthesis of the miniemulsions, an oil phase consisting of 6 g styrene, 250 mg hexadecane and 250 mg AIBN was mixed with a surfactant solution of 600 mg Lutensol AT50 in 24 g water. The mixtures were powerfully stirred at 1 500 rpm for 1 h, and the miniemulsions were prepared by pulse sonicating the emulsions for 2 min net at 90% amplitude.

The prepared non-ionic dispersions of PY74 and PV19, containing various amounts of Lutensol AT50, were used for encapsulation. To 25 g of the different pigment dispersions was, in each case, given the amount of miniemulsion that relates to the weight ratio of pigment to monomer of 80:20.

The dispersions were powerfully stirred at 1 500 rpm for 30 min, pulse sonicated for 2 min net at 50% amplitude, again stirred at 1 500 rpm for 40 min and finally pulse sonicated for 2 min net at 70% amplitude. Finally, polymerization was performed at 72 °C overnight. To achieve a complete polymerization, the gas room of the reaction flask was minimized.

Variation of the Monomer in the Encapsulation Process

The SDS-stabilized dispersion of pigment PV19 was also applied for encapsulation with polymers other than polystyrene, which was effected according to the same recipe as mentioned above (see section Synthesis of Polystyrene-Encapsulated Pigments Using Anionic Surfactant SDS and Cationic Surfactant CTMA-Cl). Encapsulating the pigment with copolymers compounded with 50 wt.-% styrene and 50 wt.-% BMA, BA, or MMA, AIBN was used for the initiation once more. However, for the homopolymerizing acrylates (BMA, BA, and MMA) in the encapsulation process, AIBN, was replaced by the same amount of oil-soluble azo initiator V-59 due to its better solubility in these monomers.

Synthesis of the Corresponding Pigment-Free Polymer Latexes

Some of the miniemulsions that were used for the various arranged pigment encapsulation processes as described before (see sections "Synthesis of Polystyrene-Encapsulated Pigments Using Anionic Surfactant SDS and Cationic Surfactant CTMA-Cl", "Synthesis of Polystyrene-Encapsulated Pigments Using Non-Ionic Surfactant Lutensol AT50", and "Variation of the Monomer in the Encapsulation Process") were polymerized in the absence of pigment in separate

DOI: 10.1002/mame.200700138

experiments. For this purpose, the produced styrene miniemulsion stabilized by SDS (see section Synthesis of Polystyrene-Encapsulated Pigments Using Anionic Surfactant SDS and Cationic Surfactant CTMA-Cl) was polymerized at 72 °C overnight. The SDS-stabilized miniemulsions containing different acrylates (BMA, BA, or MMA) or mixtures of 50 wt.-% styrene and 50 wt.-% BMA, BA, or MMA (see section Variation of the Monomer in the Encapsulation Process) were treated in the same way.

Analytical Methods

The particle diameters were measured at 25 °C using a Malvern Instruments Nano-Zetasizer at a fixed scattering angle of 173°. One droplet of dispersion was diluted with 1–1.5 mL of distilled water before measuring. Dynamic light scattering (DLS) measurements give a Z-average size (or cumulant mean), which is an intensity mean of the particle diameter, and the polydispersity index (PDI), which provides information about the width of the particle size distribution. The standard cumulant analysis is the fit of a polynomial to the log of the G1 correlation function:

$$\ln(G1) = a + bt + ct^2 + dt^3$$

The value of second order cumulant b is converted to a size using the dispersant viscosity and some instrumental constants. The coefficient of the squared term c when scaled as $2c/b^2$ is known as the polydispersity or PDI. The calculations for these parameters are defined in the ISO standard document 13321:1996 E.

The solid contents of the produced dispersions were measured gravimetrically using a Kern RH 120-3 gravimeter.

High-performance liquid chromatography (HPLC) measurements to determine the contents of monomers remaining after polymerization were performed with a Dionex HPG 680 A pump, a Dionex Acclaim 120 column (reversed phase, C18, 4.6 mm diameter, 150 mm length, 5 μm particle size, 120 Å pore size), and a Dionex UVD 170 U detector. 2 g dispersion and 100 mg of 2 wt.-% chlorobenzene as an internal standard in methanol were filled to 10 mL with methanol, resulting in flocculation of the particles. After 30 min, 2 mL were transferred over a syringe filter (PTFE membrane, 0.45 μm pore size) in an HPLC vial. 20 μL of the solution were injected. As a mobile phase (flow rate: 1.0 mL · min^{-1}), mixtures of methanol (gradient grade) and water (gradient grade) containing 0.1% acetic acid (Suprapur) were used. Within the first 5 min, the water content was decreased linearly from 60 to 40% to separate different monomers (gradient elution), then remained constant for 20 min, and finally constituted only 10% for 7 min to remove eventually the remaining non-polar substances from the column. The monomers were UV-detected at the wavelength of $\lambda = 210$ nm.

Information about the encapsulation efficiency was obtained by means of a preparative ultracentrifugation. The amount of polymer-encapsulated pigment dispersion which contained 2.5 mg polymer was put on different layered sucrose solutions with densities ranging between 1.00 and 1.30 g · cm^{-3}, the density gradient measurement was obtained by centrifugation at 4 °C for 3 h at 41 000 rpm in a Beckman L8-M ultracentrifuge. As reference, the amount of pigment-free polymer latex which contained also 2.5 mg of the same polymer material was treated in the same way. Bare polymer particles are visible in form of a white ring at low densities. To be able to quantify the encapsulation success better, there were also taken smaller amounts of polymer latexes as reference, more precisely 0.25 mg (0.025 mg) polymer correspond to a rate of 10% (1%) bare polymer in case of encapsulated samples.

For microscopic analyses [atomic force microscopy (AFM), scanning electron microscopy (SEM), transmission electron microscopy (TEM)], 1:3 diluted dispersions were dialyzed by centrifugation for 30 min at 2 500 rpm several times using a 100 000 membrane filter (exclusion volume: 100 000 g · mol^{-1}) to remove the majority of free water-soluble surfactant for a better contrast under the microscope.

Atomic force microscopy was performed with a Digital Instruments Multi Mode SPM microscope operating in tapping mode. The instrument was equipped with a Nano World monolithic silicone tip, shaped like a polygon-based pyramid, with a force constant of 42 N · m^{-1}, a resonance frequency of about 300 kHz, and a tip radius of less than 10 nm. For sample preparation, 7 μL of the dialyzed dispersion were dropped on a mica disk and a thin uniformly distributed particle layer was created via rotating the disk for 2 min at 3 000 rpm.

Scanning electron microscopy was performed with a Hitachi S-5200 FE-SEM electron microscope, operating at an acceleration voltage of 10 kV. The prepared samples were mounted on silica wafers, left to dry, and subsequently coated with platinum of 3 nm thickness.

Transmission electron microscopy was performed with a Philips EM 400 electron microscope, operating at an acceleration voltage of 80 kV. To achieve a higher resolution, measurements were also performed with a Philips CM 20 electron microscope, operating at an acceleration voltage of 200 kV. After further dilution by giving 10 μL of dialyzed samples to about 4 mL of distilled water, 3 μL were placed on a carbon-coated copper grid and left to dry. No additional contrasting was applied.

Streaming potential titrations of dispersions at different pH were done using a particle charge detector PCD 02 (Mütek GmbH, Germany). 100 mg dispersion were diluted with 100 mL hydrochloric acid containing water at pH = 3 or sodium hydroxide containing water at pH = 9. The negatively charged functional groups of 10 mL diluted dispersion were titrated with 0.001 M cationic polydiallyldimethyl ammonium chloride (PDADMAC) polyelectrolyte. For statistical reasons, each titration was repeated four times.

The polymerization kinetics was determined using a Thermal Hazard Technology μRC microreaction calorimeter. 1 g dispersion was polymerized at 72 °C. The reaction time started when adding the sample to the cell of the preheated calorimeter.

Polymer-encapsulated pigment dispersions and the corresponding pigment-free polymer latexes containing the same polymer material were freeze-dried and analyzed for their thermal behavior using a SDTA 851^{e} TGA instrument. Thereby, the samples were heated from 25 to 1 100 °C with a heating rate of 10 K · min^{-1} in nitrogen atmosphere with a gas flow of 50 mL · min^{-1}.

The molecular weights $\overline{M}_w$ of the polymers, obtained by freeze-drying the pigment-free polymer latexes, were evaluated by means of gel permeation chromatography (GPC). Depending on the solubility behavior, 10 mg of polymer were dissolved in 2 mL

THF or $CHCl_3$ and pressed through a syringe filter (PTFE membrane, pore size: 5 μm). The molecular weights were calculated with a calibration relative to polystyrene and PMMA, respectively. As molar mass distributions provided by GPC measurements depend on the polymer concentration, calibration curves were arranged using polymer solutions of the same concentration. The device for analyzing polymers that are soluble in THF consisted of a Spectra System P2000 pump, two Waters Styragel columns (each with 5 μm particle size, the first with 1 000 Å pore size, the second with 10 000 Å pore size), one PSS SDV column (5 μm particle size, 100 000 Å pore size) and a Shodex RI 71 detector. The device for analyzing polymers that are soluble in $CHCl_3$ consisted of a Dionex P580 pump, two PSS SDV columns (5 μm particle size, linear M), being located in a column furnace, and a Waters 410 RI-detector.

The glass transition temperatures of different polymers (hybrid polymers and analogous pigment-free latex polymers) were determined through DSC, using a Perkin Elmer DSC 7 instrument with a nitrogen flow of 20.0 $mL \cdot min^{-1}$ and a heating rate of 10 $K \cdot min^{-1}$ after freeze-drying the dispersions.

Results and Discussion

Different hydrophobic organic pigment nanoparticles, more precisely pigment yellow 74 (PY74), pigment violet 19 (PV19), and pigment blue 15:3 (PB15:3), were polymer encapsulated by cosonicating the corresponding nanoparticle dispersion and a monomer miniemulsion followed by polymerization (Figure 2). Oil-soluble azo initiators were used to start the radical polymerizations within the monomer droplets in order to prevent potential homogeneous nucleation in the water phase, which can lead to undesirable formation of secondary polymer particles.

In previous studies, carbon black had already been encapsulated in the same way.[19] The entire coverage of the pigments with polymer could be achieved when using only 20 wt.-% monomer, as it was shown by BET-measurements. Additionally, the encapsulation performance could be improved by cosonicating the nanoparticle dispersion and monomer miniemulsion twice, as revealed by means of TEM, ultracentrifuge experiments, and adsorption isotherms. Therefore, in this paper, all pigment encapsulations with polymer were performed using a constant pigment to monomer weight ratio of 80:20 and additional secondary sonication.

Encapsulation of Pigments with Polystyrene

In the first set of experiments, various pigment dispersions should be encapsulated with polystyrene. The used dispersions of anionically SDS-stabilized pigment PY74, PV19, and PB15:3, of cationically CTMA-Cl-stabilized PV19 and of non-ionically Lutensol-stabilized PY74 and PV19, respectively showed pigment particle diameters in the range of 100 nm with rather high PDI values, indicating broad particle size distributions (Table 1).

Ionic Stabilization

Ionically encapsulating stabilized pigment particles with polystyrene, the amount of residual monomer detected after polymerization by means of HPLC analysis is negligibly low (Table 2). For further applications, complete conversion of the monomer is essential, since many monomers such as styrene are harmful and act as swelling agent and consequently a diluent for the polymer, changing its physical properties by decreasing its glass transition temperature and hardness.

Using PY74 dispersion containing only 8.8 wt.-% of the surfactant SDS (relating to the pigment) for encapsulation with polystyrene, the diameter of the particles grows from 130 to 170 nm (NS250) during or after the process (Table 2). Increasing the surfactant content of the PY74 dispersion used for encapsulation from 8.8 to 17.6 wt.-%, the average diameter of the resulting hybrid particles can be decreased to less than 150 nm (NS260B), which nearly fits the size of pure PY74 particles. Encapsulating PV19 or PB15:3 dispersions having SDS contents of about 17 wt.-%, stable hybrid particles with almost

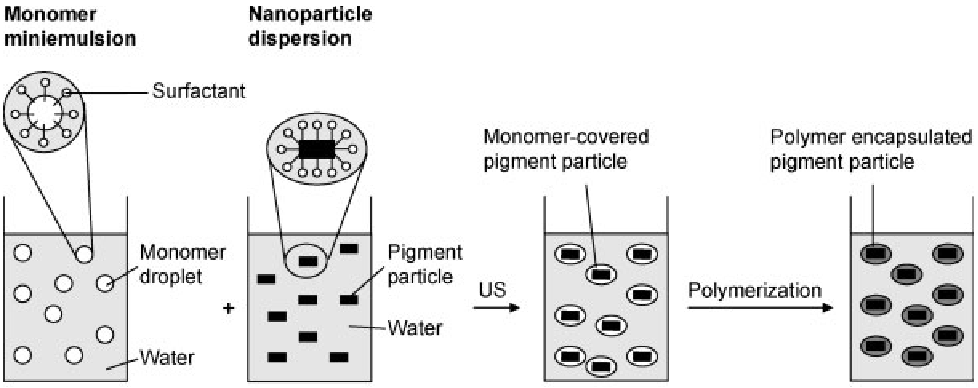

Figure 2. Principle of pigment encapsulation with polymer. In the first step, pigment particles are covered with a monomer layer adsorbed on the surface by cosonicating (US) the corresponding nanoparticle dispersion and monomer miniemulsion. In the second step, polymerization occurs, started by an oil-soluble azo initiator contained in the monomer phase. The polymerization can be described as a polymerization in an adsorbed monomer layer created and stabilized as miniemulsion ("ad-miniemulsion polymerization").

Table 2. Characteristics of the ionically stabilized pigment dispersions before and after encapsulation with polystyrene. In each case, a constant pigment to monomer weight ratio of 80:20 was used in the encapsulation process.

Dispersion	**Before encapsulation**				**After encapsulation**			
	Pigment	**Particle diameter**[a]	**PDI**[a]	**Surfactant**	**Particle diameter**[a]	**PDI**[a]	**Solid content**	**Residual styrene**[b]
		nm			**nm**		**%**	**%**
NS204	–	–	–	SDS	95	0.058	19.6	0.0
NS250	PY74 (17.0 wt.-%)[c]	132	0.316	SDS (8.8 wt.-%)[d]	169	0.300	19.5	0.1
NS260B	PY74 (17.0 wt.-%)[c]	132	0.316	SDS (17.6 wt.-%)[d]	148	0.263	20.3	0.1
NS183	PV19 (20.0 wt.-%)[c]	89	0.181	SDS (17.5 wt.-%)[d]	88	0.169	22.5	0.1
NS265B	PV19 (10.0 wt.-%)[c]	99	0.254	CTMA-Cl (25.0 wt.-%)[d]	100	0.243	12.4	0.5
NS102	PB15:3 (17.0 wt.-%)[c]	112	0.290	SDS (17.6 wt.-%)[d]	110	0.264	20.5	0.1

[a]Determined by DLS; [b]Determined by HPLC; [c]Related to total quantity; [d]Related to pigment.

the same size and size distribution as the corresponding pure pigment particles can be produced (NS183, 102), indicating that no significant particle agglomeration occurs during or after the encapsulation process. Agglomeration during the encapsulation is also not noticed on replacing the anionic surfactant SDS by the cationic surfactant CTMA-Cl (NS265B).

That no aggregation of the hybrid particles is observed during and after polymerization, can be regarded as the first indication for complete coverage of the pigment particles with polymer, as incompletely covered particles tend to agglomeration, caused by attractive London forces between the pigment particles.

However, since pigment and monomer were used for the encapsulation process in the weight ratio of 80:20, theoretical calculations result in a polymer layer with a thickness of less than 10 nm surrounding the pigment particle of the resulting hybrids, provided that complete and uniform coverage of the pigment surface is obtained. As particle diameters obtained by DLS measurements can differ by about 5–10 nm measuring dispersions twice, no conclusion about the real thickness of the polymer layer can be drawn on the basis of this measurement method.

The encapsulation efficiency was characterized by means of sedimentation experiments in a preparative ultracentrifuge. For this purpose, sucrose solutions of different densities were layered, building up a density gradient from 1.00 to 1.30 g · cm^{-3}, where low density bare polystyrene particles can be easily separated from high density pigment particles and encapsulated species with different layer thickness and perfection, respectively.

Due to the density of polystyrene ($\rho = 1.054$ g · cm^{-3}),[21] particles of SDS-stabilized pigment-free polystyrene latex (reference sample NS204, Table 2) are placed between the water phase ($\rho = 1.00$ g · cm^{-3}) and the sucrose solution with the density $\rho = 1.08$ g · cm^{-3}, visible as a white ring [see Figure 3(a), 2.5 mg of polystyrene are used]. Particles of the likewise stabilized dispersions of pigment yellow 74 [ρ(PY74) = 1.41 g · cm^{-3}; Figure 3(b)] and pigment violet 19 [ρ(PV19) = 1.47 g · cm^{-3}; Figure 3(d)] are predominantly placed at the bottom of the ultracentrifuge tubes. Some pigment particles are also located in the saturated sugar solution ($\rho = 1.30$ g · cm^{-3}), a few even more above, which can be explained by the lower density of surfactant covered pigment particles, possessing a broad particle size distribution. Ultracentrifugating polystyrene-encapsulated

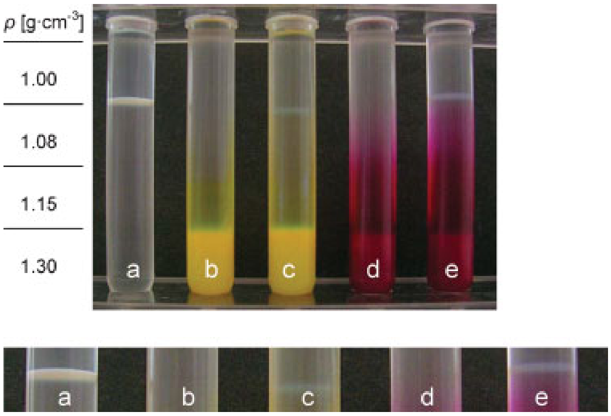

Figure 3. Top panel: density distribution of the dispersions. (a) Pure polystyrene latex (2.5 mg PS; NS204), (b) dispersion of PY74, (c) dispersion of polystyrene-encapsulated PY74 (NS250), (d) dispersion of PV19, and (e) dispersion of polystyrene-encapsulated PV19 (NS183); bottom panel: heightened polymer containing part of the centrifugation tubes. (a) Polystyrene latex (NS204), (b) dispersion of PY74, (c) dispersion of polystyrene-encapsulated PY74 (NS250), (d) dispersion of PV19, and (e) dispersion of polystyrene-encapsulated PV19 (NS183).

dispersions of pigment yellow 74 [NS250, Figure 3(c)] and pigment violet 19 [NS183, Figure 3(e)], in each case containing the same amount of polystyrene (2.5 mg) as the reference pure polystyrene latex [NS204, Figure 3(a)], a much lower intensity of the white polymer ring is detected, indicating that most of the polystyrene is indeed located on the pigment surface. The ring of the nanocomposite dispersions is about half as intensive compared to 1/10 of polystyrene particles (0.25 mg, not shown), so that one can assume that the amount of polymer not located at the pigment surface is in the range of 5%. The distribution of the nanocomposite particles in the gradient nearly corresponds to one of the analogous pure pigment particles, and merely the sucrose solution with the density $\rho = 1.08\ \text{g} \cdot \text{cm}^{-3}$ is only a little more colored. The produced hybrids contain only 20 wt.-% polymer in the solid on average, thus normally possessing slightly lower densities compared to pure pigment particles.

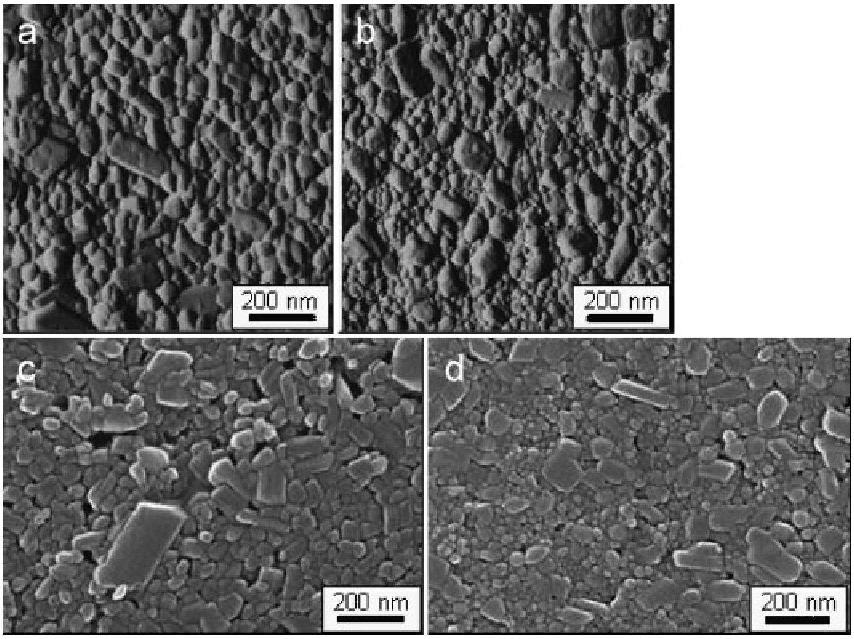

Figure 4. AFM picture of (a) PY74 pigment particles and (b) polystyrene-encapsulated PY74 particles (NS250); SEM picture of (c) PY74 particles and (d) polystyrene-encapsulated PY74 particles (NS250).

Ultracentrifugating the anionically stabilized PB15:3/polystyrene dispersion [NS102, ρ(PB15:3) = 1.61 $\text{g} \cdot \text{cm}^{-3}$] and the cationically stabilized PV19/polystyrene dispersion (NS265B), same encapsulation efficiency is found.

The centrifugation experiments show that hybrid particles are formed by this encapsulation method; however, entire coverage of the pigments with polymer cannot be proven by this measurement method. Furthermore, the existence of free uncovered pigment particles cannot be excluded that way. To obtain further information about the encapsulation efficiency, NS250 was analyzed using microscopic methods, more precisely AFM, TEM, and SEM. The yellow pigment dispersion PY74 (without polystyrene) was analyzed for comparison.

Using AFM, the height profiles of PY74 particles [Figure 4(a)] and their encapsulated pendants [NS250, Figure 4(b)] were compared. The particle size distribution of the pure pigment particles is rather broad. Small roundish particles exist next to large angled particles with a length of 100 nm and more. In comparison, the encapsulated pigment particles seem to have more rounded edges and less sharp angles. Although the differences are marginal, they at least indicate the adsorption of polymer on the particles' surface.

Same observation can be done comparing SEM pictures of the pure pigment [Figure 4(c)] with its encapsulated pendant [NS250, Figure 4(d)].

The TEM picture of pigment yellow 74 [Figure 5(a)] shows pigment particles that are often highly agglomerated, which is due to the attractive pigment–pigment interaction. Analyzing the 80:20 physical mixture of PY74 particles and pure reference polystyrene particles [NS204, Figure 5(b)], one can see bare spherical polystyrene particles with a narrow particle size distribution and diameters of about 80 nm next to pigment PY74 particles. Observing the encapsulated sample [NS250, Figure 5(c)], no bare polymer particles are visible. However, around complete particles, a layer with a lower level of optical density can be seen, especially when highly magnifying the hybrid particles [NS250, Figure 5(d)], probably revealing pigment encapsulation with polystyrene.

To further analyze whether the pigment particles are polystyrene encapsulated completely or not, streaming potential titrations of diluted NS183 and, for comparison, also anionically SDS-stabilized PV19 dispersion with 0.001 M PDADMAC, which is the chloride of a positively charged polymer, were conducted at pH = 3 and 9.

The aqueous suspension of pigment PV19 possesses a slightly negative zeta potential ζ. Within the last step of its production process, an intramolecular Friedel-Crafts acylation in polyphosphoric acid at high temperatures, the ring closing is done between the aromatic system and the carboxylic group (Scheme 1).

As traces of the acid–base active carboxylic groups remain unreacted, the particles' surface contains some

DOI: 10.1002/mame.200700138

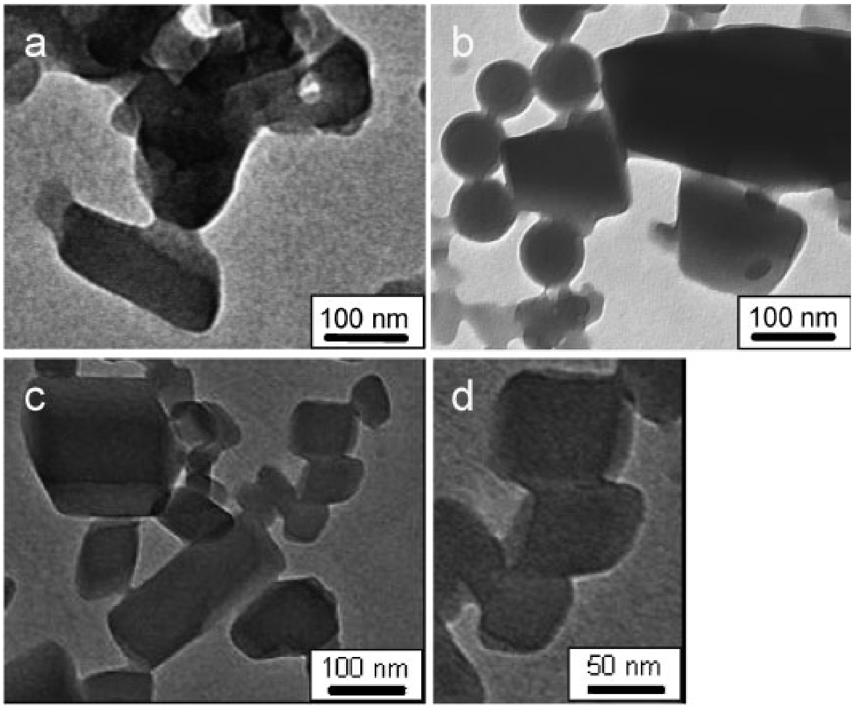

Figure 5. TEM picture of (a) PY74 particles and (b) a mixture of 80% PY74 and 20% polystyrene particles (NS204); and (c) polystyrene-encapsulated PY74 particles (NS250) and (d) highly magnified hybrid particles (NS250).

acidic groups, whereby the density of negative charges on the surface increases with growing pH, caused by deprotonation. Therefore, increasing the pH of the PV19 dispersion from 3 to 9, the particle charge density increases, too. As a consequence, the consumption of PDADMAC solution is higher when conducting a streaming potential titration of the diluted PV19 dispersion at $pH = 9$ than at $pH = 3$ (see Table 3).

Contrary to this, titrating diluted PV19/polystyrene hybrid dispersion NS183, the consumption of PDADMAC solution is identical at $pH = 3$ and 9 (Table 3), which means that the surface charge density of PV19/polystyrene nanocomposite particles does not depend on the pH value of the dispersion. If the particles were incompletely encapsulated with polymer, there would still be some carboxylic groups on the hybrid particle–water interfaces. Therefore, their surface charge density would vary with the pH value, and consequently also the PDADMAC consumption of the streaming potential titration. Since polystyrene is not acid–base active in the relevant pH corridor, the identical consumption of PDADMAC solution when titrating NS183 at different pH indicates that the surface is completely surrounded with polymer.

The influence of the kind of pigment in terms of its molecular structure on the polymerization kinetics was analyzed by means of calorimetric measurements. For this purpose, the calorimetric curves of styrene polymerization reactions taking place at the surface of pigment yellow 74 (NS250) and pigment violet 19 (NS183) particles (ad-miniemulsion polymerizations) were generated and compared with the one of a typical styrene miniemulsion polymerization in the absence of pigment (NS204, Figure 6). The polymerization was in each case initiated by the oil-soluble initiator AIBN.

The reaction course of a typical miniemulsion polymerization can be divided into three different intervals. The first interval, which is characterized by its growing polymerization rate, is the particle nucleation interval. Polymerization starts immediately and the maximum reaction rate is reached within less than 15 min. As the monomer in the droplets is continuously consumed, the second interval is characterized by an exponential decrease of the polymerization rate. After about 40 min, a weak gel peak occurs due to the increase in viscosity. Finally, reaction is complete after about 100 min.

Ad-miniemulsion polymerizations are characterized by a strongly different reaction kinetics compared to a typical

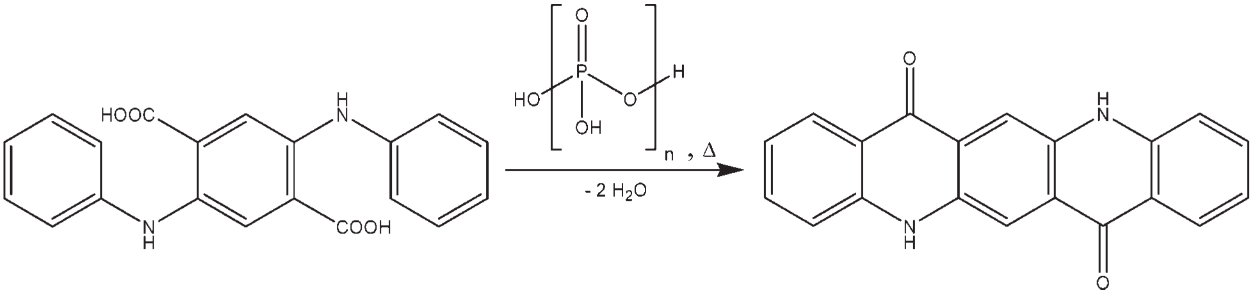

Scheme 1. Intramolecular Friedl-Crafts acylation, the last step in the production process of pigment violet 19.

Table 3. Consumption of 0.001 M PDADMAC in the streaming potential titration of 1:1 000 diluted dispersions of SDS-stabilized PV19 and NS183 (corresponding solid contents of about 0.02%) at pH = 3 and 9, respectively. The charge per surface area can be calculated out of it.

Dispersion	pH value of the dispersion during measurement	Average consumption	Standard deviation	Charge per surface area	Standard deviation
		μL	μL	$-e \cdot nm^{-2}$	$-e \cdot nm^{-2}$
PV19	3	755	24	4.96	0.16
PV19	9	865	15	5.68	0.10
NS183	3	835	15	4.91	0.09
NS183	9	835	11	4.91	0.06

miniemulsion polymerization. Conducting the polymerization on the surface of PY74 particles, the reaction rate is much lower. The maximum polymerization rate is achieved after about 1 h. As in case of the pigment-free styrene miniemulsion polymerization, an exponential decrease in the polymerization rate follows, but over a significantly longer period of time; the polymerization is not completed until about 8 h. The considerably lower reaction rate can be attributed to the existence of the nitrobenzene fragment in pigment yellow 74 molecules retarding the polymerization out of its effective scavenger effect.

For polymerizing styrene on the surface of PV19 particles, a remarkable inhibition period of about 2 h 30 min is noticed. After about further 60 min, the maximum reaction rate is achieved. An exponential decrease in the polymerization rate follows, whereas polymerization in this interval takes place much faster than in the case of reaction on the surface of PY74. The inhibition period that occurs when polymerizing styrene at the surface of pigment PV19 can be explained by its molecular structure. Pigment PV19 as unsubstituted *trans*-quinacridone has a molecular structure similar to quinonoid compounds such as benzoquinones, which generally are strong inhibitors of polymerization reactions.

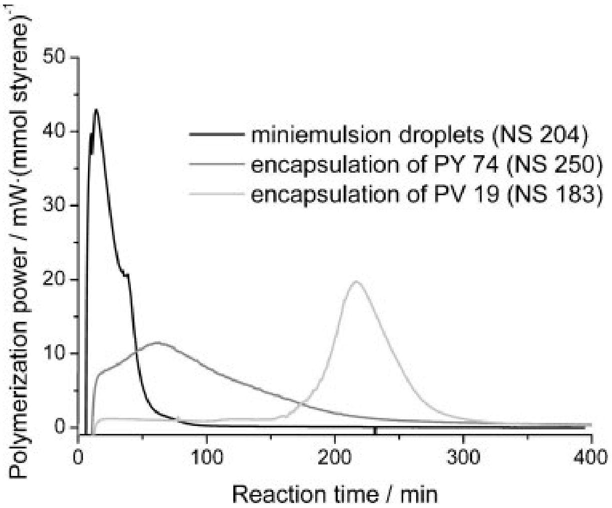

Figure 6. Calorimetric curves of styrene polymerizations taking place on the surface of the pigments PY74 (NS250) and PV19 (NS183) (ad-miniemulsion polymerizations) and comparison with the kinetics of a typical styrene miniemulsion polymerization (in the absence of pigment, NS204); the polymerization was in each case started by the oil-soluble initiator AIBN.

Regarding the calorimetric curves of the polymerizations taking place on the surface of pigment yellow 74 and pigment violet 19, no gel peak is apparent. This can be attributed to the fact that the polymerization takes place in a thin monomer layer with a thickness of presumably clearly less than 10 nm (and consequently of low volume) adsorbed on the pigment surface.

Summarized, reaction kinetics of ad-miniemulsion polymerizations, proceeding on pigment particles' surface, is not only affected by the mere existence of pigment particles but also in particular by their molecular structure that can cause retardation or an inhibition period for the polymerization. Moreover, the influence of the pigments' molecular structure on the reaction course of the polymerization can be seen as further indication for the existence of adsorbed monomer layers, and therefore finally also for polymer encapsulation.

Non-Ionic Stabilization

The pigments PV19 and PY74 can also be encapsulated with polystyrene using the non-ionic surfactant Lutensol AT50. As in the case of ionic stabilization, with about 0.1%, the amount of residual monomer detected after polymerization through HPLC analysis is negligibly low (Table 4).

However, compared to ionic surfactants, higher amounts of surfactant have to be applied to stabilize the dispersions during the encapsulation process. As just mentioned, only about 17 wt.-% of ionic surfactants like SDS or CTMA-Cl can prevent particle agglomeration completely during the encapsulation process. Using the non-ionic surfactant Lutensol AT50, efficient stability was only obtained for surfactant contents of at least 30 wt.-%. Even then, distinct agglomeration is still noticed as the significant increase in particle size during the

DOI: 10.1002/mame.200700138

Table 4. Characteristics of different Lutensol AT50-stabilized pigment dispersions before and after encapsulation with polystyrene. In each case, a constant pigment to monomer weight ratio of 80:20 was used in the encapsulation process.

Dispersion	Before encapsulation					After encapsulation			
	Pigment	Particle diameter[a]	PDI[a]	Pigment content[b]	Surfactant content[c]	Particle diameter[a]	PDI[a]	Solid content	Residual styrene[d]
		nm		wt.-%	wt.-%	nm		%	%
NS255C	PY74	143	0.242	9.9	30.0	273	0.245	12.9	0.1
NS255D	PY74	143	0.242	9.8	40.0	247	0.252	14.1	0.1
NS255E	PY74	143	0.242	9.7	50.0	244	0.275	15.1	0.2
NS263A	PY74	143	0.242	9.2	100.0	229	0.279	18.9	0.1
NS259A	PV19	94	0.211	10.0	30.0	215	0.224	13.0	0.2
NS262A	PV19	94	0.211	10.0	40.0	205	0.211	14.0	0.1
NS259B	PV19	94	0.211	10.0	50.0	177	0.197	16.9	0.2
NS259E	PV19	94	0.211	10.0	100.0	168	0.196	21.4	0.1

[a]Determined by DLS; [b]Related to total quantity; [c]Related to pigment; [d]Determined by HPLC.

encapsulation process shows (see Table 4). The apparent lower efficiency of non-ionic surfactants like Lutensol AT50 compared to the just-mentioned ionic pendants with respect to the weight fraction can be reasoned by the fact that about the same surface area has to be stabilized by a far longer non-ionic oligomeric chain.

Thereby, the higher the surfactant contents of the inserted pigment dispersions, and therefore the higher the density of stabilizing surfactant on the particles' surface, the less agglomeration occurs. Agglomeration, and consequently the increase in particle size, is more pronounced encapsulating pigment violet 19 (NS259A, B, E, 262A) than pigment yellow 74 (NS255C-E, 263A), which might be explained by the lower particle diameters and therefore larger surface area per weight of PV19 to be stabilized by surfactant during the encapsulation compared to PY74.

The encapsulation efficiencies were analyzed by ultracentrifugating in each case the amount of hybrid dispersion containing 2.5 mg of polystyrene. As reference, different amounts of pure polystyrene latex (NS 204) were treated in an analogous manner. Independent of the Lutensol content, all PY74/polystyrene hybrid dispersions contain almost no bare polystyrene particles, more precisely the amount of polymer not located at the pigment surface is estimated to be 1%, whereas the amount of bare polymer particles increases from about 1 (NS259E) to 10% (NS262A, 259B) with decreasing amount of applied surfactant when PV19 is encapsulated. Using only 30 wt.-% surfactant compared to the pigment (NS259A), clearly more than 10% of the polymer is not located at the pigment particles' surface. Here, the agglomeration tendency resulting in larger sizes of the final particles correlates with the encapsulation efficiencies.

Variation of the Monomer

Since the success of encapsulation depends on various physical and chemical parameters such as adsorption enthalpies and specific interactions, the change in monomer composition was also investigated. Thereby, one can moreover utilize the diverse properties of the finally produced hybrid polymers.

The encapsulation of PV19 with low T_g polymers, such as PBMA (NS230) and PBA (NS242), were successfully achieved. Encapsulating PV19 with PMMA (NS238), the polarity of the magenta particles' surface can be increased. Surrounding the pigment with various copolymers built from 50 wt.-% styrene and 50 wt.-% BMA (NS219), BA (NS227), or MMA (NS224), one can combine the properties of polystyrene with those of the corresponding polyacrylates. Copolymerizing styrene with different acrylates in bulk, the reactivity ratios r are determined to be $r_{STY} = 0.56$ and $r_{BMA} = 0.40$ for the copolymerization with BMA,[22] $r_{STY} = 0.698 \pm 0.033$ and $r_{BA} = 0.164 \pm 0.017$ for the copolymerization with BA[23] and finally $r_{STY} = 0.520 \pm 0.026$ and $r_{MMA} = 0.460 \pm 0.026$ for the copolymerization with MMA.[24] As the reactivity ratios of the comonomers are of the same dimension, rather homogeneous polymer structures should be obtained by copolymerizing mixtures of 50 wt.-% styrene and 50 wt.-% of the just mentioned acrylates. In all the cases, the dispersions were anionically stabilized by using SDS as the surfactant.

Table 5. Analytical data of different PV19/polymer hybrid dispersions. The hybrid dispersions were obtained by encapsulating SDS-stabilized dispersion of PV19 (particle diameter: 89 nm, PDI: 0.181, pigment content: 20.0 wt.-%, surfactant content: 17.5 wt.-%) with various polymers, using a constant pigment to monomer weight ratio of 80:20.

Dispersion	Polymer material	Particle diameter[a)] nm	*PDI*[a)]	Solid content %	Residual styrene[b)] %	Residual acrylate[b)] %
NS183	Polystyrene	88	0.169	22.6	0.1	–
NS230	PBMA	94	0.163	23.5	–	0.2
NS242	PBA	100	0.187	22.8	–	0.6
NS238	PMMA	167	0.181	22.9	–	0.5
NS246	PMMA[c)]	91	0.184	10.0	–	0.7
NS219	Poly(BMA-*co*-STY)[d)]	89	0.176	22.9	0.1	0.2
NS227	Poly(BA-*co*-STY)[d)]	90	0.169	23.2	0.0	1.0
NS224	Poly(MMA-*co*-STY)[d)]	93	0.160	22.8	0.1	0.4

[a)] Determined by DLS; [b)] Determined by HPLC; [c)] Here, the PV19 dispersion was diluted 1:1 with water, resulting in a pigment content of 10.0 wt.-%, before usage for encapsulation; [d)] Compounded of 50 wt.-% styrene and 50 wt.-% of the corresponding acrylate.

Encapsulating pigment violet 19 with the just-mentioned polymer materials, the amount of residual monomer, acting as diluent for the polymer, detected after polymerization is in each case negligibly low (Table 5), as just realized for the encapsulation with polystyrene (NS183). With the exception of the PV19/PMMA nanocomposites (NS238), the produced hybrid particles have about the same size and size distribution as the pure pigment particles (see Table 5), which can be reasoned by the high efficiency of the low molecular ionic surfactant SDS and the assumed complete polymer coverage of the particles, as already intensely explained for the PV19/polystyrene hybrids (NS183). However, the particle diameter of the PV19/PMMA nanocomposites is almost doubled during the encapsulation. The particle aggregation processes can be explained by attractive interactions between the polar MMA layers located on the surface of different pigment particles. These interactions can be avoided by diluting the PV19 dispersion by 1:1 with water, leading to a pigment content of only 10 wt.-%, prior to polymer encapsulation. In this way, hybrids with an average particle size of 91 nm can be produced (NS246).

The encapsulation performance was analyzed by means of ultracentrifugation of the hybrids and, for comparison and rough quantification, different amounts of the pigment-free polymer latexes containing the same polymer materials. The particles of the pure polymer latexes are located between the layers of density $\rho = 1.00$ and $1.08\ \mathrm{g \cdot cm^{-3}}$ in the case of polystyrene (NS 204), PBMA (NS236), PBA (NS245), poly[(butyl methacrylate)-*co*-styrene] (NS216), and poly[(butyl acrylate)-*co*-styrene] (NS223). In contrast, PMMA (NS237) and poly[(methyl methacrylate)-*co*-styrene] particles (NS222) are localized on the interface between the layers of density 1.08 and $1.15\ \mathrm{g \cdot cm^{-3}}$. Pure PMMA has a density of about $\rho = 1.19\ \mathrm{g \cdot cm^{-3}}$ (20 °C).[21] The lower density of the synthesized PMMA nanoparticles can be explained by the influence of hexadecane ($\rho = 0.77\ \mathrm{g \cdot cm^{-3}}$ at 20 °C) and the surfactant. As there are some hybrid particles within the layers of density $\rho = 1.08$ and $1.15\ \mathrm{g \cdot cm^{-3}}$, it is particularly difficult to estimate the amount of bare PMMA particles. The amount of pure polymer particles (which are not located at the pigment surface) is in the range of 5% in case of PV19/homopolymer hybrid dispersions (NS183, 230, 238, 242, 246) and in the range of 1% in case of PV19/copolymer hybrid dispersions (NS219, 224, 227). Obviously, both styrene and different acrylates are suited for the stabilization of the quinacridone pigment surface very well. It is presumed that the aromatic quinacridone practices attractive π–π interactions with styrene and can interact with the acrylates through London forces. Beyond, the formation of charge transfer complexes between quinacridone and monomer molecules is also conceivable.

By means of thermo-gravimetric analysis (TGA), the composition of the PV19/polymer hybrids was determined. The thermograms of the freeze-dried hybrid dispersions reveal three steps: a first at 230 °C for hexadecane/SDS, a second at about 400 °C for the polymer (Table 6), and a third at 565 °C for the pigment. The step heights of the hybrids' thermograms approximately correspond to the calculated ones that are obtained considering the encapsulation recipe and thermal behavior of the hybrids' single components.

Furthermore, the presumed interactions between the quinacridone pigment and the various polymers, more precisely attractive London forces, π–π interactions and

DOI: 10.1002/mame.200700138

Table 6. Thermal decomposition data of different hybrid polymers. The hybrids were obtained by encapsulating SDS-stabilized dispersion of PV19 with various polymers, using a constant pigment to monomer weight ratio of 80:20, and analyzed by TGA after freeze-drying. For comparison, the corresponding pigment-free polymer latexes were treated in the same way.

Polymer material	**PV19/polymer hybrid dispersion**			**Pigment-free polymer latex**	
	Dispersion	**Inflexion point**[a)]	**Mass loss**[a)]	**Dispersion**	**Inflexion point**[a)]
		°C	**%**		**°C**
Polystyrene	NS183	420	16	NS204	417
PBMA	NS230	385	17	NS236	338
PBA	NS242	388	14	NS245	399
PMMA	NS238	418	17	NS237	372
Poly(BMA-*co*-styrene)[b)]	NS219	394	15	NS216	426
Poly(BA-*co*-styrene)[b)]	NS227	393	14	NS223	406
Poly(MMA-*co*-styrene)[b)]	NS224	409	14	NS222	401

[a)]Polymer decomposition, apparent in the decomposition curve obtained by TGA analysis; [b)]Compounded of 50 wt.-% styrene and 50 wt.-% of the corresponding acrylate.

may be even charge transfer complexes can ensure, that the thermal behavior of a hybrid is not exactly consistent with the thermal behavior of a simple mixture of its constituents. Next to the slight deviations in the decomposition step height of some hybrid polymers from the calculated values, this can also explain the observation that the height of the hybrids' pigment decomposition step is clearly lower than expected at the correspondingly unexpected high percentage on residue, likely basically carbon. This phenomenon might additionally be reasoned by the reaction of initiator radicals with quinacridone through the addition or chain transfer to polymerization-inactive radicals during the inhibition period of the polymerization, which also influences the thermal behavior of the pigment. Consequently, one can assume that the real composition of the hybrids approximately corresponds to the theoretical one, in particular that the hybrids' weight ratio of pigment to polymer amounts to about 80:20.

Due to strong (adsorptive) interactions between the pigment and the polymer, the PV19/polymer hybrids could not be separated in their constituents, the pigment and the surrounding polymer, by using usual solvents. Therefore, only the molar mass distribution of the corresponding freeze-dried pigment-free polymer latexes was evaluated by GPC. However, one has to be aware that the reaction kinetics of ad-miniemulsion polymerizations taking place at the surface of PV19 clearly differs from the reaction course of typical miniemulsion polymerizations, as just noticed for the example of styrene polymerization. Both the existence and molecular structure of the pigment have an influence on the reaction kinetics, and consequently also on the molecular weight of the resulting polymer. The molecular weights $\overline{M}_w$ of polystyrene (NS204) and the already mentioned copolymers (NS216, 222, 223) amount to about 250 000 to 400 000 $g \cdot mol^{-1}$, those of the polyacrylates (NS236, 237, 245) are about 10^6 $g \cdot mol^{-1}$.

The glass transition temperatures of the hybrid polymers were measured by means of DSC. Depending on the kind of monomer (mixture) being polymerized on the pigment particles' surface, the glass transition temperature of the resulting polymer can be varied between −45 and +106 °C. Polymerizing monomer on the crystalline magenta pigments' surface tends to result in slightly higher glass transition temperatures compared to polymerization in pigment-free miniemulsion droplets (see Table 7), probably out of the assumed higher molecular weights of the hybrid polymers compared to their pigment-free pendants. Moreover, amorphous parts of semicrystalline polymers often possess increased T_g values compared to their non-crystalline pendants out of the neighboring crystallites restricting the molecular-motion by steric constraint. Accordingly, it is possible, that the crystalline magenta pigment influences the T_g of the hybrid polymers in an analogous manner. The glass transition temperatures of the various produced hybrid and pigment-free polyacrylates agree well with the values found in literature.[21] Only in the case of polystyrene, the glass transition temperatures of the produced polymers (NS183, 204) are nearly 20 K lower than that in literature.[21] However, by omitting the hydrophobe hexadecane in the synthesis of pure polystyrene latex under otherwise same conditions, the T_g can be increased to 98 °C, indicating that hexadecane acts as a plastifier for polystyrene. Polymerizing monomer mixtures, one can create homogeneous copolymers with glass transition temperatures anywhere between those of the corresponding homopolymers.

Table 7. Glass transition temperature of different hybrid polymers. The hybrids were obtained by encapsulating SDS-stabilized dispersion of PV19 with various polymers, using a constant pigment to monomer weight ratio of 80:20, and analyzed by DSC after freeze-drying. For comparison, the corresponding pigment-free polymer latexes were treated in the same way.

Polymer material	**PV19/polymer hybrid dispersion**		**Pigment-free polymer latex**	
	Dispersion	**T_g (polymer)**	**Dispersion**	**T_g (polymer)**
		°C		**°C**
Polystyrene	NS183	85	NS204	82
PBMA	NS230	35	NS236	30
PBA	NS242	−45	NS245	−47
PMMA	NS238	106	NS237	103
Poly(BMA-*co*-styrene)[a]	NS219	48	NS216	49
Poly(BA-*co*-styrene)[a]	NS227	29	NS223	20
Poly(MMA-*co*-styrene)[a]	NS224	95	NS222	83

[a] Compounded of 50 wt.-% styrene and 50 wt.-% of the corresponding acrylate.

Conclusion

Different organic pigment nanoparticles can be encapsulated efficiently with polymer resulting in hybrid structures with the weight ratio of pigment to polymer of 80:20 by cosonicating the corresponding pigment dispersion and a monomer miniemulsion, as shown in the example of polystyrene encapsulation of pigment particles stabilized by anionic SDS, cationic CTMA-Cl, or non-ionic Lutensol AT50. Encapsulation was proven by a combination of analytic methods, including ultracentrifugation, electron microscopic methods, and streaming potential titrations at different pH values.

Comparing the reaction kinetics of a typical styrene miniemulsion polymerization (in the absence of pigment) with the corresponding ad-miniemulsion polymerizations proceeding on different pigment particles' surface, one notices an influence of the kind of pigment in terms of its molecular structure. The considerably lower reaction rate when polymerizing styrene on the surface of PY74 particles can be attributed to the existence of the nitrobenzene fragment in pigment PY74 molecules, retarding the reaction as an effective scavenger. The remarkable inhibition period of the analogous reaction on PV19's surface can also be attributed to its molecular structure. PV19 molecules as unsubstituted *trans*-quinacridones are characterized by their similarity to quinonoid compounds, which generally act as strong inhibitors of polymerization reactions.

Besides polystyrene, the quinacridone pigment particles were also successfully encapsulated with different polyacrylates and with copolymers composed of units of styrene and the corresponding acrylates. Thermograms of the hybrids reveal three steps which fit the decomposition of SDS/hexadecane, the polymer and the pigment, and indicate that the real composition of the hybrids approximately corresponds to the theoretical one, in particular that the nanocomposites' weight ratio of pigment to polymer amounts to about 80:20. The glass transition temperature of the polymer on the pigment surface can be well adjusted by the composition of the polymer material. Hybrid polymers tend to possess a little higher T_gs compared to the corresponding pigment-free polymer latex particles, probably out of their assumed higher molecular weights or the neighboring pigment crystallites.

Acknowledgements: We would like to thank *Clariant AG*, especially Dr. *Carsten Plueg*, for providing the pigment dispersions, for a fruitful cooperation, many discussions, and financial support.

Received: May 4, 2007; Revised: July 18, 2007; Accepted: July 19, 2007; DOI: 10.1002/mame.200700138

Keywords: emulsion polymerization; encapsulation; kinetics (polym.); miniemulsion polymerization; pigments; polymerization kinetics

[1] E. Bourgeat-Lami, *J. Nanosci. Nanotech.* **2002**, *2*, 1.
[2] J.-L. Luna-Xavier, A. Guyot, E. Bourgeat-Lami, *J. Colloid Interface Sci.* **2002**, *250*, 82.
[3] P. Espiard, A. Guyot, *Polymer* **1995**, *36*, 4391.
[4] Y. Haga, T. Watanabe, R. Yosomiya, *Angew. Makromol. Chem.* **1991**, *189*, 23.
[5] L. Quaroni, G. Chumanov, *J. Am. Chem. Soc.* **1999**, *121*, 10642.

[6] E. Bourgeat-Lami, J. Lang, *J. Colloid Interface Sci.* **1998**, *197*, 293.
[7] E. Bourgeat-Lami, J. Lang, *J. Colloid Interface Sci.* **1999**, *210*, 281.
[8] E. Bourgeat-Lami, J. Lang, *Macromol. Symp.* **2000**, *151*, 377.
[9] I. Sondi, T. H. Fedynyshyn, R. Sinta, E. Matijević, *Langmuir* **2000**, *16*, 9031.
[10] K. Landfester, *Macromol. Symp.* **2000**, *150*, 171.
[11] K. Landfester, N. Bechthold, S. Förster, M. Antonietti, *Macromol. Rapid Commun.* **1999**, *20*, 81.
[12] S. Lelu, C. Novat, C. Graillat, A. Guyot, E. Bourgeat-Lami, *Polym. Int.* **2003**, *52*, 542.
[13] N. Bechthold, F. Tiarks, M. Willert, K. Landfester, M. Antonietti, *Macromol. Symp.* **2000**, *151*, 549.
[14] B. Erdem, E. D. Sudol, V. L. Dimonie, M. S. El-Aasser, *J. Polym. Sci., Part A: Polym. Chem.* **2000**, *38*, 4419.
[15] B. Erdem, E. D. Sudol, V. L. Dimonie, M. S. El-Aasser, *J. Polym. Sci., Part A: Polym. Chem.* **2000**, *38*, 4431.
[16] B. Erdem, E. D. Sudol, V. L. Dimonie, M. S. El-Aasser, *J. Polym. Sci., Part A: Polym. Chem.* **2000**, *38*, 4441.
[17] D. Hoffmann, K. Landfester, M. Antonietti, *Magnetohydrodynamics* **2001**, *37*, 217.
[18] F. Tiarks, K. Landfester, M. Antonietti, *Langmuir* **2001**, *17*, 5775.
[19] F. Tiarks, K. Landfester, M. Antonietti, *Macromol. Chem. Phys.* **2001**, *202*, 51.
[20] L. P. Ramírez, K. Landfester, *Macromol. Chem. Phys.* **2003**, *204*, 22.
[21] "*Polymer Handbook*", J. Brandrup, E. H. Immergut, Eds., 3rd edition, J. Wiley & Sons, New York 1989.
[22] T. Otsu, T. Ito, M. Imoto, *J. Polym. Sci., Part B: Polym. Lett.* **1965**, *3*, 113.
[23] G. Kaszás, T. Földes-Berezsnich, F. Tüdős, *Eur. Polym. J.* **1984**, *20*, 395.
[24] F. M. Lewis, C. Walling, W. Cummings, E. R. Briggs, F. R. Mayo, *J. Am. Chem. Soc.* **1948**, *70*, 1519.